Chapter 19
Imaging Objects with Coded Apertures, Utilising a Laser Wakefield X-Ray Source

M. P. Selwood, R. Heathcote and C. D. Murphy

Abstract Laser wakefield acceleration (LWFA) (Tajima and Dawson, P Rev Lett 43:267–270, 1979, [1]) is able to generate GeV electrons in millimetres of under dense plasma (Leemans et al., Nat Phys 2:696–699, 2006, [2]) due to the high fields which may be sustained. The electron beam is smaller than those from linear accelerators, and as such these bunches can be used to create hard X-ray imaging sources with micron resolution capability. The conventional pinhole imaging technique results in systems where improved resolution comes at the cost of flux reduction. At low flux, the resultant decrease in signal to noise ratio must be overcome by either a more powerful X-ray source or an increased integration time. Here, coded apertures are proposed as a viable imaging alternative for pinhole apertures without such adjustments. The imaging capabilities of coded apertures will be discussed and simulation results will be presented from ray-tracing algorithms.

19.1 Introduction

Laser wakefield acceleration (LWFA) is capable of generating femtosecond duration high energy X-ray sources with a micron-scale source size [3]. This allows for imaging systems capable of capturing still images from a rapidly evolving object with micron resolution. However, conventional pinhole imaging techniques are designed around the inverse correlation between the signal-to-noise ratio and resolution capability. To resolve 5 μm features on a typical 5 × 5 mm CCD chip, the open area ratio, and thus the throughput ratio, would be *ca*. 8×10^{-7}. This would necessitate a higher power source or long integration time; the former being costly, and the latter negating the ability to capture still images of a transient object.

M. P. Selwood (✉) · C. D. Murphy
Department of Physics, York Plasma Institute, University of York,
York YO10 5DQ, UK
e-mail: matthew.selwood@york.ac.uk

R. Heathcote
Central Laser Facility, STFC Rutherford Appleton Laboratory,
Didcot, Oxon OX11 0QX, UK

M. Kozlová and J. Nejdl (eds.), *X-Ray Lasers 2018*, Springer Proceedings
in Physics 241, https://doi.org/10.1007/978-3-030-35453-4_19

Instead a coded aperture can be used. These are an array of pinholes in specific arrangements, which each cast an image of the object onto the detector; the resultant signal from each overlaid image is dubbed the hologram. This needs to be decoded post-capture to form a likeness of the object. Coded apertures allow for a flux increase, as there are multiple pinholes, without resolution loss, as the individual pinholes are small in area. Using the MURA configuration [4] (discussed below), an open aperture area ratio of 0.5 is attainable. This is 6 orders of magnitude higher than the standard pinhole for the system described previously, and can still utilise the strobed nature of the LWFA source.

19.2 Image Decoding

A likeness of the object is decoded from the hologram via cross correlation algorithm; a quantitative measure of similarity between two signals as a function of lag [5]. Large values in the resultant array denote areas of high correlation between the two signals. For the coded aperture system, the two signals being compared are D and G; the hologram on the detector plane, and some decoding function, respectively, where the latter is constructed from the aperture design, A. These are decoded to form a likeness of the object, S, thus [4, 5]:

$$\begin{aligned}\hat{S}[i', j'] &= D[i, j] \star G[i, j] \\ &= \sum_{i'=0}^{i_{max}} \sum_{j'=0}^{j_{max}} D^*[i', j'] \cdot G[i' + i, j' + j]\end{aligned} \tag{19.1}$$

where D^* is the complex conjugate of D. Equation 19.1 can be visualised as a moving dot product; a window, G, is scanned across static array, D, and the dot product of the overlap is computed.

19.3 Coded Apertures

Under the assumption of intrinsic errors within the decoding process, combined with the fact that the detector plane is constructed such that $D = S \star A$, (19.1) becomes

$$\hat{S} = S \star (A \star G + N \star G) \tag{19.2}$$

where N is some noise term that is quasi-uniform across all spaces. In an idealised scenario, $\hat{S} = S$. For this to be reflected mathematically, G must be constructed such that $A \star G = \delta$, and $N \star G$ must equal 0. This is achieved by making G unimodular (values of ± 1) as a function of A, with a uniform density [6] to ensure that any superposition of G upon N within the moving dot product also has an expectation

value of 0. This allows the technique to be uniform background subtractive, making it favourable for high noise environments. Furthermore, this may increase the SNR by a theorised factor of up to $\sqrt{\kappa}$, where κ is the number of perforations [7].

As G is constructed from A, thus A must also have a uniform perforation density. This will also reduce imaging bias between different regions of the field of view. Errors within $A \star G$ can arise if there is translational symmetry within the design, as the superposition would then show false correlation. Thus, the aperture design cannot hold translational symmetry, or have a constant perforation separation. This is achieved through similar techniques to pseudo-noise sequencing, with a prime number basis forming the aperture dimensions, p.

19.4 Modified Uniformly Redundant Arrays (MURA)

The MURA system is capable of creating numerous aperture designs, henceforth referred to as 'masks'. A is defined by a binary array, where a value of 1 denotes a perforated element, and 0 opaque sites. A and G have been created in accordance with the equations generated by Gottesman and Fenimore [4], and examples of different p basis apertures can be seen in their paper. An experimental advantage of these designs is the presence of column $A_0 = 0$, and row $A_0 = 1$, save for the first value. Upon cyclic permutation to bring the 0th row and column to the centre, a fiducial 'cross-hair' is created through the centre of the design for detector alignment.

One other the main advantage of coded aperture imaging is that they are uniform background subtractive, as G is unimodular by design. This is shown within Fig. 19.1; decoded point sources 19.1d,e are virtually identical and possess only a 11% SNR decrease, even though the latter hologram includes a uniform background level of 70%. In contrast, if a pinhole aperture were used, the SNR degradation would be 88%, equivalent to the visual difference between holograms 19.1a, b.

As (19.1) is a comparison of two arrays, it can be seen that a scaling factor will need to be applied to the size of G in order for the features to correlate with those on the detector. The scaling factor is applied to both the i and j coordinates, and is calculated thus:

$$M_T = \frac{A_{pix}}{D_{pix}} + \frac{v}{u} + 1 \tag{19.3}$$

where A_{pix} is the desired size of any single pinhole, v is the distance between the aperture and the detector, u is the distance from aperture to object, and the ratio between them is the magnification ratio, M_R. In an experimental system, the specific aperture design required is dictated by M_R, detector dimensions (D_{len}), and A_{pix} [8]:

$$p > A_{pix}\left[\frac{2D_{len}}{D_{pix}(M_R + 1)} - 1\right] \tag{19.4}$$

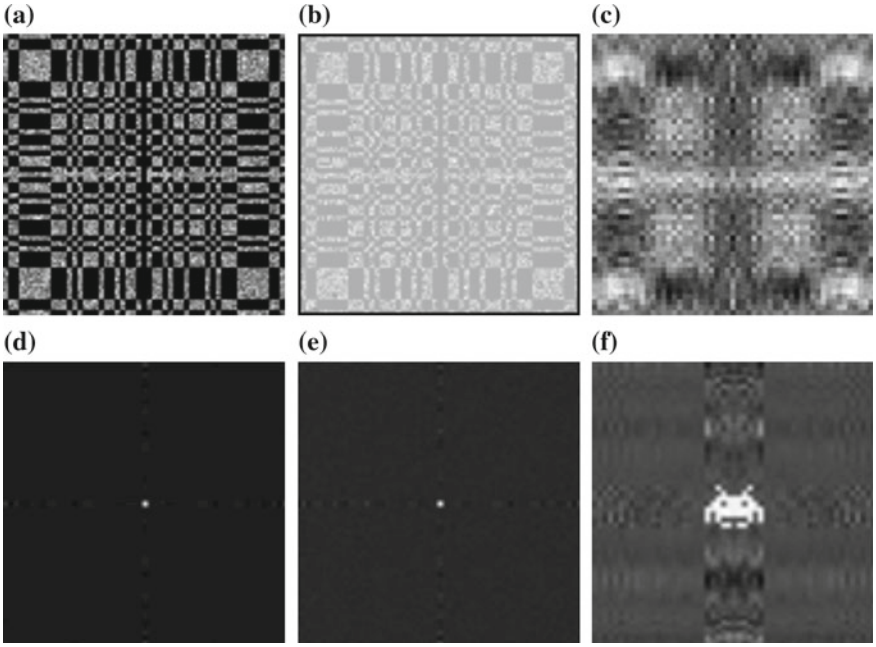

Fig. 19.1 Simulation results for a $p = 53$ aperture onto an idealised detector with $M_R = 1$, using 1×10^7 rays per point source. Holograms (**a**–**c**) were decoded to produce images of the point source, (**d**) and (**e**), and the extended object, (**f**). **b** is generated from (**a**), with the addition of a uniform background at 70% peak signal strength. **d** and **e** have an SNR of 60.1 and 53.4, respectively

where p is the smallest prime number that satisfies this criterion, and A_{pix} will be a function of the desired image resolution. As the MURA is a system of pinholes, it stands to reason that the resolution attainable would follow the same principles as that of a single pinhole [8]:

$$\frac{1}{R} = A_{pix}\left(\frac{1}{M_R} + 1\right) \tag{19.5}$$

where R is the resolution capability in the plane of the observed object, measured as the number of sources that can be resolved per unit length. As with the MURA's predecessor, the Uniformly Redundant Array (URA), the MURA possesses a theoretically quantifiable SNR [4, 9].

19.5 Simulating Holograms

A ray-tracing algorithm has been used to generate simulated holograms for decoding. A random ray, r is evaluated to see at what scalar extrapolation, τ, it crosses the plane of the aperture:

$$\tau = \frac{(\vec{P}_a - \vec{P}_s) \cdot \vec{n}}{\vec{r} \cdot \vec{n}} \tag{19.6}$$

where P_a is the position of the centre of the aperture, P_s is the position of the source, and n is the vector normal to the plane of the aperture, all in a constant reference frame. If τ is non-zero, the impact point of r on the aperture, P_i can be calculated:

$$\vec{P}_i = \vec{P}_s + \tau\, \vec{r} \tag{19.7}$$

If P_i is within the given aperture dimensions, it is compared against the binary sequence of A to test if the impact is a perforation site. All rays that are enabled to pass the aperture plane undergo (19.6) and (19.7) once more, using the position of the detector, P_d and its dimensions instead of the aperture. The number of rays impacting on each pixel of the detector can then be summed, and D built.

19.6 Conclusion

In conclusion, coded apertures are a viable imaging technique to fully utilise the improved resolution capabilities of laser wakefield acceleration X-ray sources. They are able to conserve resolution capabilities of conventional pinhole methods whilst drastically increasing the SNR. Their properties have been presented, and a ray-tracing methodology for hologram construction.

Acknowledgements This work was supported by the Engineering and Physical Sciences Research Council grants [EP/L01663X/1] and [EP/R512230/1], Scitech Precision, and the Science and Technology Facilities Council.

References

1. T. Tajima, J.M. Dawson, P. Rev. Lett. **43**, 267–270 (1979)
2. W.P. Leemans et al., Nat. Phys. **2**, 696–699 (2006)
3. S.P.D. Mangles et al., Nature **431**, 535–538 (2004); C.G.R. Geddes et al., Nature **431**, 538–541 (2004); J. Faure, et al., Nature **431**, 541–544 (2004)
4. S.R. Gottesman, E.E. Fenimore, Appl. Opt. **28**, 4344–4352 (1989)
5. A. Papoulis, *The Fourier Integral and Its Applications* (McGraw-Hill, New York, 1962)
6. E.E. Fenimore, T.M. Cannon, Appl. Opt. **17**, 337–347 (1978)
7. R.H. Dicke, Ap. J. **153**, L101–L106 (1968)

8. R. Heathcote et al., *Proceedings of SPIE Optical Engineering + Applications, San Diego*, vol 10763 (San Diego, CA, 2018), pp. 107630U-1–107630U-8
9. E.E. Fenimore, Appl. Opt. **22**, 3562–3570 (1978)